

## RESEARCH ARTICLE

# Src42A is required for E-cadherin dynamics at cell junctions during *Drosophila* axis elongation

Lenin Chandran<sup>1</sup>, Wilko Backer<sup>2</sup>, Raphael Schleutker<sup>2</sup>, Deqing Kong<sup>3</sup>, Seyed A. H. Beati<sup>1</sup>, Stefan Luschnig<sup>2,\*</sup> and H.-Arno J. Müller<sup>1,\*</sup>

## ABSTRACT

Src kinases are important regulators of cell adhesion. Here, we have explored the function of Src42A in junction remodelling during *Drosophila* gastrulation. Src42A is required for tyrosine phosphorylation at bicellular (bAJ) and tricellular (tAJ) junctions in germband cells, and localizes to hotspots of mechanical tension. The role of Src42A was investigated using maternal RNAi and CRISPR-Cas9-induced germline mosaics. We find that, during cell intercalations, Src42A is required for the contraction of junctions at anterior-posterior cell interfaces. The planar polarity of E-cadherin is compromised and E-cadherin accumulates at tricellular junctions after Src42A knockdown. Furthermore, we show that Src42A acts in concert with Abl kinase, which has also been implicated in cell intercalations. Our data suggest that Src42A is involved in two related processes: in addition to establishing tension generated by the planar polarity of MyoII, it may also act as a signalling factor at tAJs to control E-cadherin residence time.

**KEY WORDS:** *Drosophila*, Germband extension, Gastrulation, E-cadherin, Src kinase, Phosphorylation, Cell junctions

## INTRODUCTION

Gastrulation represents a crucial morphogenetic process in early embryogenesis by which the blastomeres acquire cell fates in three different germ layers and the principal body axes become established (Williams and Solnica-Krezel, 2017). Much of the cellular basis of gastrulation movements is well known from studies in model organisms, including *Drosophila melanogaster* (Gheisari et al., 2020; Paré and Zallen, 2020). In *Drosophila* the anterior-posterior (AP) pattern originates during oogenesis to set up molecular gradients in the fertilized egg, which inform the elongation of the AP axis in a process called germband extension. The translation of the AP patterning into directional movement of the germband critically involves the generation of planar cell polarity through Toll-like receptor proteins (Paré et al., 2014).

A band of ventral-lateral epidermal cells forms the germband, which, during gastrulation, more than doubles its length along the

anterior-posterior axis of the embryo, while narrowing in the dorsal-ventral direction (Kong et al., 2017). The cell behaviours associated with the extension of the germband include rearrangements of the apical cell contacts and basolateral cell protrusions (Sun et al., 2017). Three different modes of cell intercalations involving the apical cell junctions have been described: T1 transition, multiple rosette formation and vertex sliding (Bertet et al., 2004; Blankenship et al., 2006; Vanderleest et al., 2018). All three behaviours require the adherens junctions (AJs) to undergo precisely controlled remodelling (Levayer and Lecuit, 2013; Levayer et al., 2011; Rauzi et al., 2010). According to their position within the blastoderm epithelium, AJs can be classified into bicellular junctions (bAJs), referring to a two-cell interface, and tricellular junctions (tAJs), referring to a cell vertex where three cells attach to each other; both bAJs and tAJs are modulated during germband elongation.


The T1 transition describes the intercalation between four cells that exchange their neighbours by shrinking the bAJs in vertical direction and extending a new junction in horizontal direction (Bertet et al., 2004). The localized contraction and extension of the bAJ is facilitated through a planar polarized distribution of non-muscle myosin II (MyoII), the levels of which are enriched at vertical (anterior/posterior, AP) cell interfaces, while the scaffolding protein Bazooka (Baz) along with the E-cadherin/catenin complex is enriched at the horizontal (dorsoventral, DV) interfaces (Kong et al., 2017; Paré and Zallen, 2020; Zallen and Wieschaus, 2004). Interference with the planar polarization of either of these proteins negatively affects cell intercalation. For example, disruption of AP patterning via *Krüppel* RNAi knockdown affects junctional remodelling and MyoII AP planar polarity (Bertet et al., 2004). Junctional remodelling is also dependent on tyrosine phosphorylation. For example, the DV planar polarity of  $\beta$ -catenin is compromised after Abelson (Abl) tyrosine kinase knockdown (*abl<sup>l</sup>*), resulting delayed cell intercalations (Tamada et al., 2012).

More recent studies have shown that tAJs also play a role in germband extension. The transmembrane protein Sidekick (Sdk) exclusively localizes at the tAJs and is vital for maintaining the length of the AP and DV interfaces. *sdk* mutants show defects in apical vertex adhesion and less strain in the tissue, resulting in a reduced rate of T1 transition (Finegan et al., 2019). In addition, Sdk localization changes with increasing mechanical tension. Expression of Myosin light chain phosphatase resulted in reduced Sidekick accumulation at the tAJs, suggesting that Sidekick protein levels are controlled by mechanical tension (Letizia et al., 2019). More recently, it has been shown that Canoe and its vertex localization are vital for cell intercalation; the translocation of Canoe from the tAJs to bAJs is crucial for germband extension, and this mobilization is mediated by phosphotyrosine signalling through Abl kinase (Yu and Zallen, 2020).

In addition to Abl, Src kinases have also been shown to be involved in germband elongation. A first report provided evidence

<sup>1</sup>Developmental Genetics, Institut für Biologie, Universität Kassel, 34132 Kassel, Germany. <sup>2</sup>Institute for Integrative Cell Biology and Physiology, Cells in Motion Interfaculty Centre, Westfälische Wilhelms Universität Münster, 48149 Münster, Germany. <sup>3</sup>Developmental Genetics, Fachbereich Biologie, Philipps Universität Marburg, 35037 Marburg, Germany.

\*Authors for correspondence (h.a.muller@uni-kassel.de; luschnig@uni-muenster.de)

 S.A.H.B., 0000-0002-8104-2362; S.L., 0000-0002-0634-3368; H.-A.J.M., 0000-0002-7525-6874

that Src42A, in conjunction with the small GTPase Rac1, is required for the formation of actin-rich protrusions on the basal side of multicellular rosettes (Sun et al., 2017). Src42A was shown to be a component of a signalling pathway mediating the cell surface information from Toll-2 receptors towards PI3-kinase in order to promote the formation of MyoII planar polarity (Tamada et al., 2021). However, despite the well-known functions of Src family kinases in cell adhesion, the role of Src42A in regulating the distribution and dynamics of the E-cadherin adhesion complex has not yet been studied.

In this study we have explored the function of one of the two Src kinases encoded in the *Drosophila* genome, *Src42A*, in fine-tuning tAJs and bAJs during T1 transition. Consistent with previous reports, we find that Src42A has a substantial impact on T1 transitions. After Src42A single knockdown (*Src42A<sup>i</sup>*), the contraction of the AP border and the planar polarity of the bAJs are impaired. The delayed T1 transitions in *Src42A<sup>i</sup>* embryos led to slower cell intercalation, and correlated with reduced tension at the AP cell border and a delay in the rate at which the AP borders shrink during T1 transition. *Src42A<sup>i</sup>* embryos exhibit increased E-cadherin levels at the AP cell border, suggesting that the turnover of E-cadherin is affected. Consequently, E-cadherin intensity at the tAJs is increased in intercalating cells. E-cadherin dynamics at tAJs show an accumulation and dispersion cycle, which is affected by reducing the level of Src42A. Our data suggest that Src42A is involved in two not mutually exclusive processes; in addition to its function in Toll-2-like receptor signalling instructing the planar polarity of MyoII, we propose that it also acts as a signalling factor in controlling the amount of time that E-cadherin is present at tAJs.

## RESULTS

### Dynamic association of Src42A with plasma membrane domains in the early embryo

The *Drosophila* genome encodes two Src homologs: Src42A and Src64B. To detect endogenous Src42A protein, we generated an antiserum against a full-length GST-Src42A fusion protein. The antibody was used to examine protein levels in embryos zygotically mutant for the loss-of-function allele *Src42A<sup>26-1</sup>* (Takahashi et al., 2005). Src42A levels were significantly reduced in late-stage embryos homozygous for *Src42A<sup>26-1</sup>* compared with heterozygous controls. At gastrulation stages, Src42A protein levels were unimpaired between homozygous and heterozygous *Src42A<sup>26-1</sup>* embryos, and were markedly reduced only at late stages of embryogenesis (Fig. 1A,B; Fig. S1A-E). Immunostaining of embryos expressing HA-tagged Src42A or Src64B revealed that the antibody was specific for *Src42A*, and did not crossreact with Src64B (Fig. S2). We conclude that our Src42A antibody detects maternally provided Src42A protein that decreases during embryogenesis, but persists at low levels into late stages of embryonic development.

Consistent with earlier studies, we found that Src42A exhibits a differential and dynamic association with plasma membrane domains in the early embryo from cellularization onwards (Takahashi et al., 2005). In early to mid-cellularization, Src42A was localized at the apical aspect of the growing plasma membrane, where it partially colocalized with Baz at the plasma membrane cortex (Fig. 1C,C'). A second accumulation of Src42A protein was present at the basal tip of the furrow canal, where the localization overlapped with Myo II (Fig. 1C,C'). During late cellularization, when spot AJs move apically, Src42A accumulated at the emerging apical AJs, whereas levels of Src42A at the furrow canals decreased (Fig. 1C,C'). During gastrulation, Src42A was observed at bAJs and tAJs on the apical side of the lateral epidermis during germband

extension. (Fig. 1D,D'; Fig. S3A-C). Src42A was slightly enriched at the AP interface, where Myo II was localized during the generation of planar cell polarity (Fig. 1D'; Fig. S3D,E). We conclude that, by using a specific antibody, we detected a differential localization of Src42A at distinct plasma membrane domains in early embryos. The observation that Src42A was especially enriched at tension-generating sites prompted us to examine the function of Src42A during gastrulation.

### Maternal knockdown of Src42A affects embryogenesis from the blastoderm stage onwards

Gastrulation stage embryos that are homozygous mutant for *Src42A<sup>26-1</sup>* harbour considerable amounts of maternal Src42A protein (Fig. S1E). The elimination of maternally supplied Src42A is not possible using the conventional autosomal DFS-FRT technique, as the *Src42A* locus is present between the centromere and the most proximal available FRT site (Chou and Perrimon, 1996). Therefore, to deplete maternal Src42A, RNAi knockdown experiments were conducted by employing the UAS/GAL4 system to express a transgenic short hairpin RNA using the *P{TRiP.HMC04138}* line (Brand and Perrimon, 1993; Staller et al., 2013) (Fig. 2A).

Embryos expressing *TRiP04138* showed reduced hatching rates with variable penetrance and expressivity, depending on the maternal Gal4 driver used (Fig. 2A'). A combination of *P{mat $\alpha$ 4-GAL4-VP16}67*; *P{mat $\alpha$ 4-GAL4-VP16}15* [called *mat67* (*mat15* hereafter)] was most efficient as embryos showed about 80% reduction in hatching rates and were therefore used for all the experiments (called *Src42A<sup>i</sup>* in this study). At late syncytial and early cellular blastoderm stages, 40% of *Src42A<sup>i</sup>* embryos exhibited a defect in cytoplasmic clearing indicated by an irregular interface between the central yolk and the clear cortical cytoplasm (Fig. 2B,D; Movie 1). By immunoblotting, we found that embryos with clearing defects exhibited the most severe reduction in Src42A protein levels (Fig. 2C). Similar clearing defects have also been reported for embryos injected with dsRNA against Src42A mRNA (Sun et al., 2017). *Src42A<sup>i</sup>* embryos displayed variable cuticle phenotypes, which were stronger compared with zygotic *Src42A<sup>26-1</sup>* homozygous mutants (Fig. 2E).

Although the *Src42A<sup>i</sup>* embryos did not exhibit major defects at the onset of gastrulation movements, defects in cytoplasmic clearing suggest a requirement for Src42A in cellularization, which may lead to an abnormal blastoderm epithelium in the knockdown embryos. We therefore examined the localization of markers for membrane domains during cellularization and found no major differences of *Src42A<sup>i</sup>* embryos compared with controls (Fig. S4). Despite the formation of a rather normal blastoderm epithelium, we found that occasionally nuclei dropped from the cell cortex into the centre of the embryo during early cellularization (Fig. S4B; Movie 1). We conclude that *Src42A<sup>i</sup>* embryos exhibit mild cellularization defects, including cytoplasmic clearing and nuclei dropping from the cortex, but that the overall polarized structure of the blastoderm epithelium remains largely unimpaired.

### Src42A is required for germband extension and for normal phosphotyrosine levels at bAJs and tAJs

Our results showed that maternal Src42A is required for embryogenesis, but that the depletion of maternal Src42A only causes minor defects in the formation of the blastoderm. We found by immunofluorescence that during germband extension Src42A was localized at bAJs and tAJs (Fig. 1B; Fig. S3). bAJ- and tAJ-resident proteins have been reported to undergo dynamic

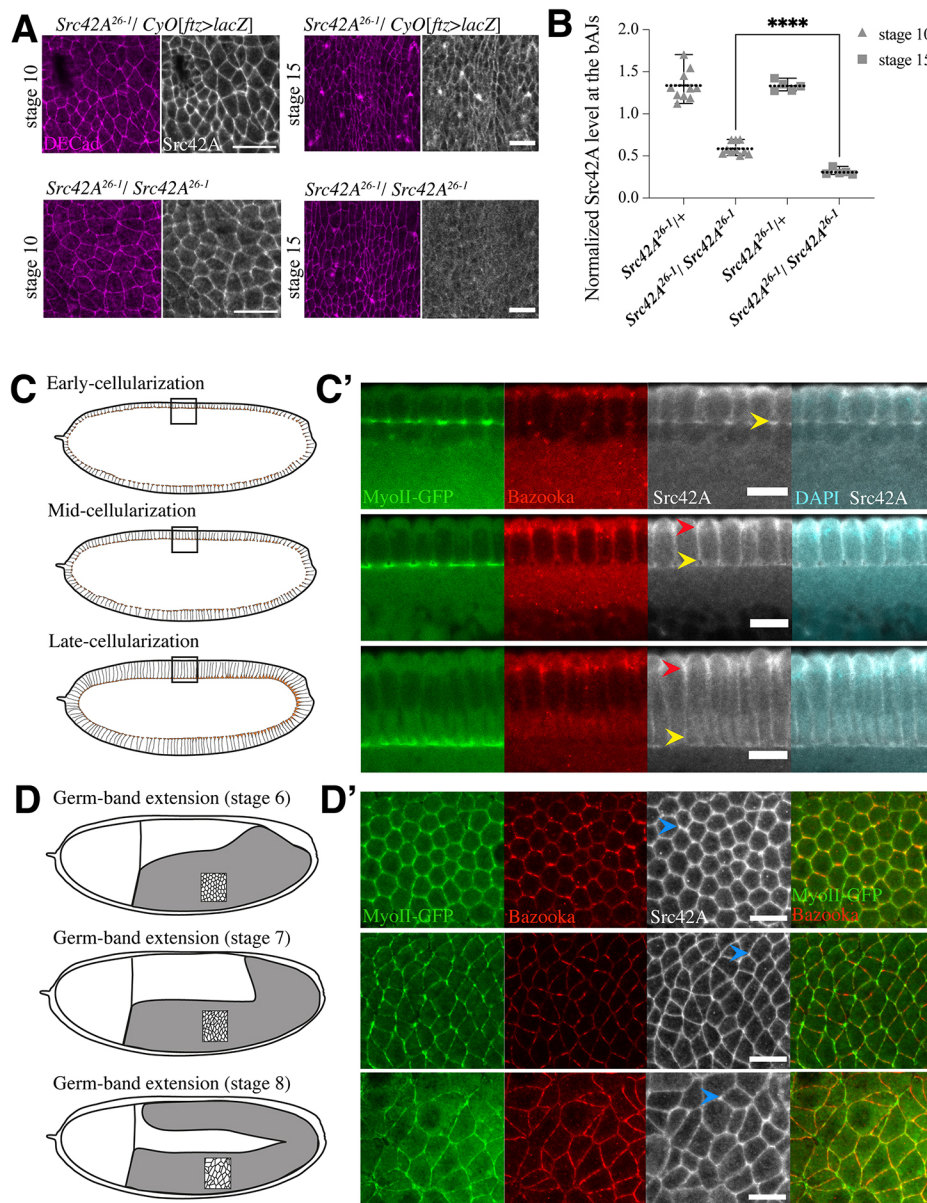


**Fig. 1. Subcellular localization of Src42A during cellularization and germband extension.** (A) Confocal imaging of heterozygous *Src42A<sup>26-1</sup>/CyO[ftz>lacZ]* and homozygous *Src42A<sup>26-1</sup>/Src42A<sup>26-1</sup>* embryos stained for E-cadherin (magenta) and Src42A (grey). Embryonic stages are indicated on the left. (B) Maternal Src42A quantification at bicellular adherens junctions in stage 10 and stage 15 embryos. The plotted values represent Src42A fluorescence intensities normalized to E-cadherin intensity. Each data point (a grey triangle or square) in the graph corresponds to an average pixel intensity measurement from 10 cell junctions in a single embryo. Dotted line represents the mean; error bars indicate the range of the minimum and maximum values (\*\*\*\* $P < 0.0001$ ; paired Student's *t*-test). (C,D) Schematics of cellularization and germband extension stages corresponding to the stages in C', D'. (C', D') Confocal micrographs of *MyoII::KI-GFP* (Ambrosini et al., 2019) cellularization stage (transverse sections) and germband extension stage (surface projection) embryos. Embryos were fixed and immunostained for Bazooka (red), Src42A (grey), DAPI (cyan) and MyoII-GFP (green). Arrowheads indicate the furrow canal (yellow, C'), adherens junction (red, C') and cell vertex (blue, D'). Scale bars: 10  $\mu$ m.

redistribution during germband extension (Finegan et al., 2019; Uechi and Kuranaga, 2019). *Src42A<sup>i</sup>* embryos exhibit defects in germband elongation, when analysed by video time-lapse recordings (Fig. 3A; Movie 2). Germband elongation occurs in two phases: an initial fast phase, in which the germband doubles its length within 25 min at 25°C, is followed by a slow phase with an additional 0.5-fold elongation within 70 min (da Silva and Vincent, 2007; Irvine and Wieschaus, 1994) (Fig. 3B,C). Plotting of cumulative displacement length of the germband over time revealed a substantial delay in its AP extension (Fig. 3B). Germband cells showed a 0.25- and 0.16-fold delay in *Src42A<sup>i</sup>* embryos for the fast and for the slow phase, respectively (Fig. 3C-E). We further examined germband cells in *Src42A<sup>i</sup>* embryos at a subcellular level. Src42A has several known substrates, which are present at bAJs and tAJs (Brunet et al., 2013; Takahashi et al., 2005). Indeed, at the onset of germband extension (stage 7), *Src42A<sup>i</sup>* embryos exhibited significantly reduced phosphotyrosine levels at bAJs and tAJs (Fig. 3F-H). This indicates that Src42A is required for normal levels of protein phosphorylation at tyrosine residues at

bAJs and tAJs. Consistent with earlier findings that Src42A controls germ band elongation by changing the properties of signalling factors at the subcellular level (Sun et al., 2017; Tamada et al., 2021), these results demonstrate that Src42A-dependent tyrosine phosphorylation is required for normal germband elongation.

### Src42A is required for normal timing of T1 transitions

T1 transitions are a key cell behaviour during the fast phase of germband extension. It involves junction contraction at the AP cell interfaces followed by neighbour exchange along the DV axis, resulting in tissue elongation (Bertet et al., 2004). Recently, it was shown that Src kinases play a role downstream of Toll-2 in planar polarization of Myosin II and Baz (Tamada et al., 2021); when both Src42A and Src64B were knocked down, the rate of intercalation determined by altered arbitrary cell edge contraction rates was reduced. Based on the finding that *Src42A<sup>i</sup>* embryos display drastic reduction in the fast phase of germband elongation (Fig. 3D), we sought to investigate T1 transitions in *Src42A<sup>i</sup>* embryos. Using Utrophin-GFP as a marker for the plasma membrane-associated

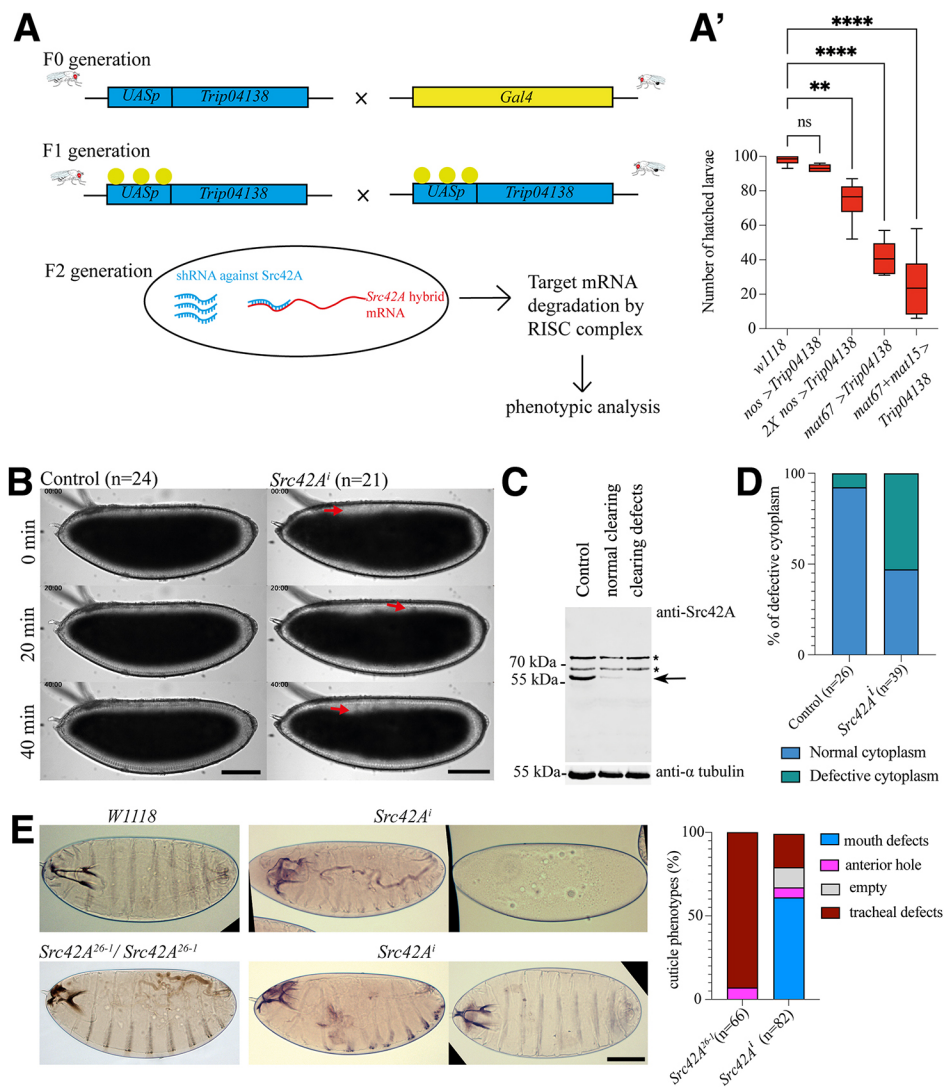


**Fig. 2. Characterization of Src42A knockdown.** (A) Crossing scheme for Src42A knockdown using the UAS/GAL4 system.

*Trip04138* expresses short hairpin RNA (blue) against endogenous Src42A mRNA (red). *Gal4* is shown in yellow. (A') Src42A knockdown analysis using different maternal *Gal4* driver lines. Significance was tested using Dunnett's multiple comparison test. The boxes indicate the interquartile range; whiskers indicate the range of the minimum and maximum values; the horizontal lines indicate the median. ( $n=300$ ).  $P=0.8788$  (ns) for *nos > Trip04138*,  $**P=0.0043$  for  $2Xnos > Trip04138$ ,  $****P=0.0001$  for *mat67 > Trip04138* and  $****P=0.0001$  for *mat67 + mat1.5 > Trip04138*.

(B) Bright-field images showing the cytoplasmic clearing defect during the cellularization stage in *Src42A<sup>i</sup>* compared with control embryos (red arrows indicate clearing defects) (Movie 1). (C) Western blot analysis of *Src42A<sup>i</sup>* embryos. Cellularization stage embryos (15 each) showing clearing defects and normal clearing from *Src42A<sup>i</sup>* crosses were selected, lysed and subjected to SDS-PAGE and western blot analysis. Embryos with clearing defects show a strong reduction in Src42A protein levels (~59 kDa is marked with an arrow). As a loading control, the same blot was re-probed with an antibody against  $\alpha$ -tubulin (~55 kDa). The anti Src42A antibody also recognized two nonspecific bands (marked by asterisks).

(D) The percentages of clearing defects were calculated based on the total  $n$  values (number of embryos). (E) Representative larval cuticles derived from wild-type (*w<sup>1118</sup>*), *Src42A* zygotically mutant (*Src42A<sup>26-1</sup>/Src42A<sup>26-1</sup>*) and *Src42A<sup>i</sup>* embryos. Four classes of phenotype were identified and their relative distributions in the two conditions were quantified. Scale bars: 100  $\mu$ m.

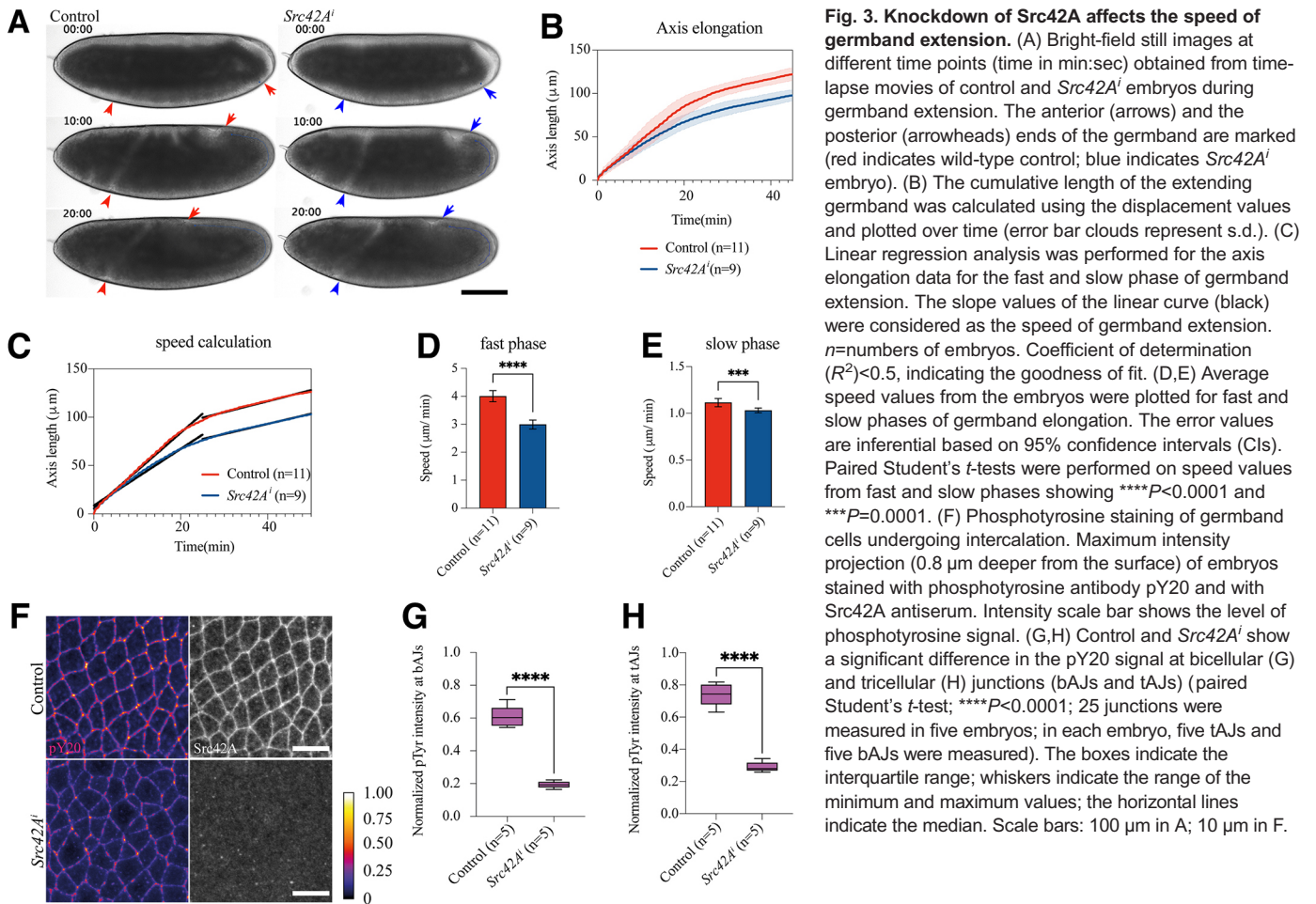
actin cortex, T1 transitions were recorded in control and *Src42A<sup>i</sup>* embryos (Movie 3). The shrinkage of the junction was measured as the time it takes for the AP interface junction between two adjacent vertices on the DV axis to shrink into a single four-cell vertex. In four-cell vertices undergoing T1 transitions, the shrinking junction along the AP axis reduces its length with an average of 1.25 min (Fig. 4A). When compromising *Src42A* function, this aspect of the T1-process was delayed (Fig. 4B). In 60% of the cases in the *Src42A* knockdown, the shrinking of the AP junction interface was not completed after 2 min (Fig. 4B',D). This suggests that the rate at which T1 transitions occur is delayed due to less contractility at the AP junctions. We noted that the number of germband cells in *Src42A<sup>i</sup>* embryos was slightly decreased and the average apical cell area was larger than in wild-type controls (Fig. S5). These defects may be related to the nuclear dropping observed during cellularization in *Src42A<sup>i</sup>* embryos. However, it is unlikely that these effects cause the delay in T1 transitions, as cell size and cell number were shown to have little if any effect on germband extension (Edgar and O'Farrell, 1989; Irvine and Wieschaus, 1994). We conclude that *Src42A* is required for contraction of AP junctions during T1 transitions in germband elongation.

In T1 transitions, the AP cell border is enriched with MyoII, which mediates tension through its contractile properties. Moreover,

a supracellular enrichment of MyoII was also reported to occur due to tensile forces along the AP cell interfaces (Bertet et al., 2004; Fernandez-Gonzalez et al., 2009). In *Src42A*, *Src64B* double-knockdown embryos, MyoII planar polarity was reduced (Tamada et al., 2021). We found that, in single-knockdown *Src42A<sup>i</sup>* embryos T1 transitions are delayed and we asked whether this correlates with a reduction in MyoII-dependent tension at the AP border of the cells undergoing T1 transition. To measure the tension at the AP cell boundaries, we performed laser ablation experiments in intercalating cells and measured the recoil velocity. When the AP border was cut, the detached tAJs moved slower in *Src42A<sup>i</sup>* embryos compared with control (Fig. 5A). The displacement of tAJs was normalized to initial length and plotted over time (Fig. 5B,C). A non-linear regression analysis on the displacement data revealed that the initial recoil velocity was reduced in T1 transitions in *Src42A<sup>i</sup>* embryos (Fig. 5D). From these experiments, we conclude that Src42A is involved in generating or maintaining tension in intercalating cells at T1 transitions.

#### Src42A acts in concert with Abl in controlling E-cadherin and $\beta$ -catenin levels at the AP cell interfaces

In *Drosophila*, Src42A genetically interacts with components of the E-cadherin/ $\beta$ -catenin complex and Src42A can be detected in a



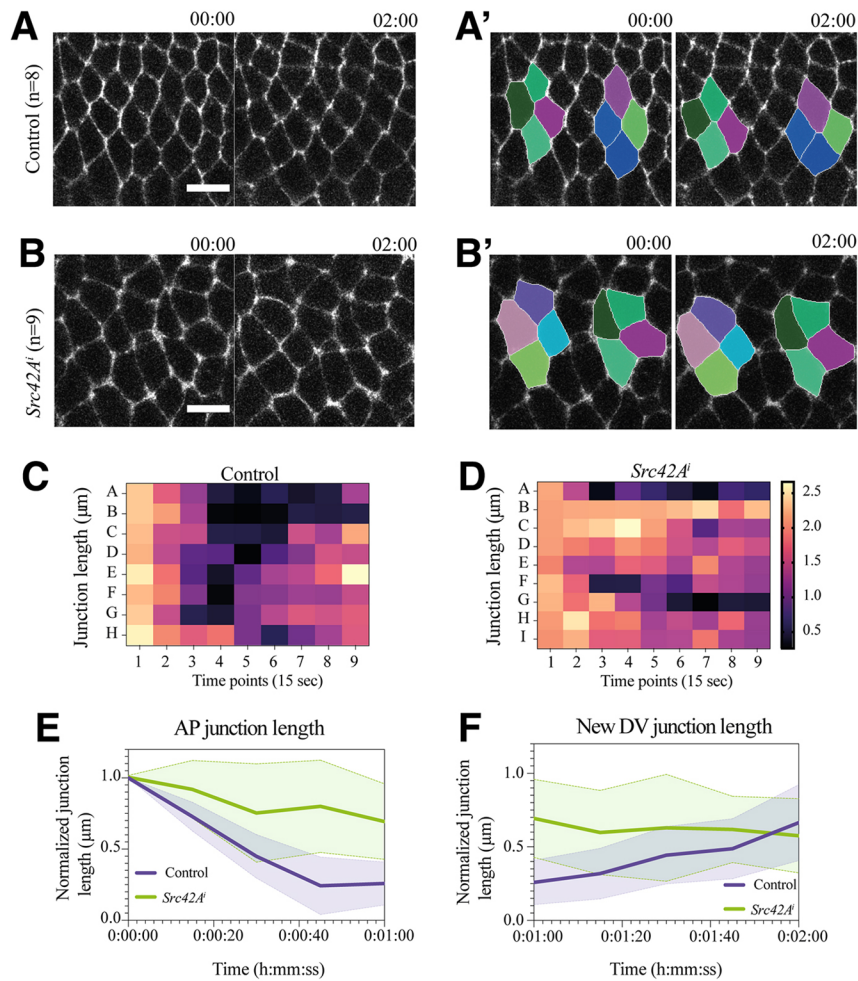
ternary complex with E-cadherin and  $\beta$ -catenin (Takahashi et al., 2005). Furthermore, the adhesive properties of the mammalian E-cadherin-catenin complex are regulated by phosphorylation of Y654 of  $\beta$ -catenin through c-src (Röper et al., 2018).  $\beta$ -Catenin exhibits a planar-polarized distribution and is preferentially localized at the DV cell border of germband cells; the phosphorylation of  $\beta$ -catenin Y667 by Abelson kinase (Abl) is vital to achieve this polarization (Tamada et al., 2012). It has also been shown in the *Drosophila* wing epithelium that *Src42A* can potentially activate Abl kinase (Singh et al., 2010). These data raised the hypothesis that *Src42A* affects the E-cadherin/ $\beta$ -catenin complex indirectly via Abl. In *Src42A*<sup>1</sup> embryos, there was no significant change in protein levels at the DV cell border, but the AP borders showed enhanced levels of  $\beta$ -catenin and E-cadherin (Fig. 6). These data were also supported by quantification of live imaging of E-cadherin-GFP in wild-type and *Src42A*<sup>1</sup> embryos (Fig. S6). We conclude that the planar polarity of the E-cadherin-catenin complex is compromised in *Src42A*<sup>1</sup> embryos (Fig. 6A-E).

To examine the relationship of *Src42A* and Abl in axis extension, we conducted a double knockdown experiment targeting both kinases. Germband elongation was examined by time-lapse video microscopy in controls compared with single knockdowns and *Src42A*<sup>1</sup>+*Abl*<sup>1</sup> double knockdowns (Fig. 7). The cumulative displacement values were plotted over time and the speed of elongation was calculated from the displacement data (Fig. 7A-C). We found that, in the initial fast phase, *Src42A*<sup>1</sup>+*Abl*<sup>1</sup> exhibits a slightly stronger delay in germband extension than *Src42A*<sup>1</sup> or *Abl*<sup>1</sup>

alone; *Abl*<sup>1</sup> alone did not affect the speed of germband elongation in the fast phase (Fig. 7B,C). During the slow phase of extension, *Src42A*<sup>1</sup>+*Abl*<sup>1</sup> showed stronger delay compared with *Src42A*<sup>1</sup> or *Abl*<sup>1</sup> alone (Fig. 7B,C). As the overall effect on germband extension in *Abl*<sup>1</sup> single knockdowns was rather mild (Fig. 7A-C), we examined Abl protein levels in *Abl*<sup>1</sup> embryos and found that Abl protein was still detectable at bAJs, indicating perdurance of maternal Abl protein (Fig. 7D,D'). Although *Src42A* levels were unimpaired in *Abl*<sup>1</sup> knockdown embryos, Abl protein was slightly reduced in *Src42A*<sup>1</sup> embryos (Fig. 7E-F'). These data indicate that *Src42A* and *Abl* are both required for germband extension. As *Src42A* is required for normal bAJ localization of Abl, we propose that, similar to the cell invasion process in the wing imaginal disc epithelium (Singh et al., 2010), *Src42A* may act upstream of Abl in a common pathway.

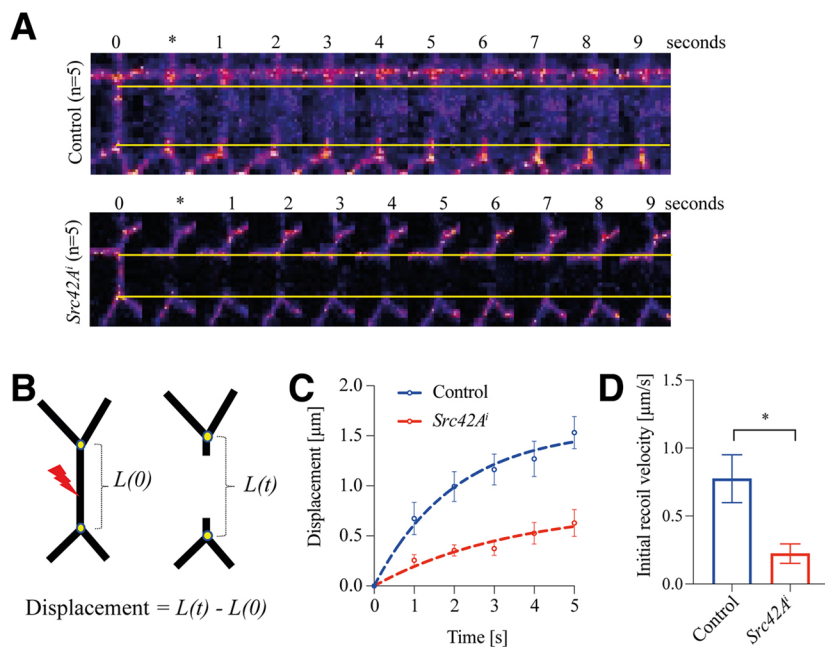
### ***Src42A* controls E-cadherin turnover at tAJs during T1 transitions**

We found that *Src42A* showed a distinct accumulation at the tAJs (Fig. 1B). The tAJs is one of the tension hotspots during germband elongation, and Sidekick (Sdk) protein is a core component of this subcellular domain (Finegan et al., 2019; Salomon et al., 2017; Uechi and Kuranaga, 2019). Sdk also regulates E-cadherin endocytosis during cell intercalation when new junction formation occurs at the horizontal interface (Letizia et al., 2019). Despite the requirement of Sdk, the mechanisms controlling E-cadherin dynamics at the tAJs are not well understood. Therefore, we



recorded E-cadherin-GFP localization in the background of *Src42A<sup>1</sup>* during T1 transition. The localization of E-cadherin-GFP exhibits an accumulation and dispersion cycle during T1 transition at tAJs (Fig. 8A) (Vanderleest et al., 2018). In *Src42A<sup>1</sup>* embryos, E-cadherin

levels were continuously increasing at the tAJs, suggesting that the turnover of E-cadherin is affected during T1 transition (Fig. 8A; Movie 4). From the vertex intensity ratio calculation, E-cadherin levels were not fluctuating in embryos deficient for *Src42A*



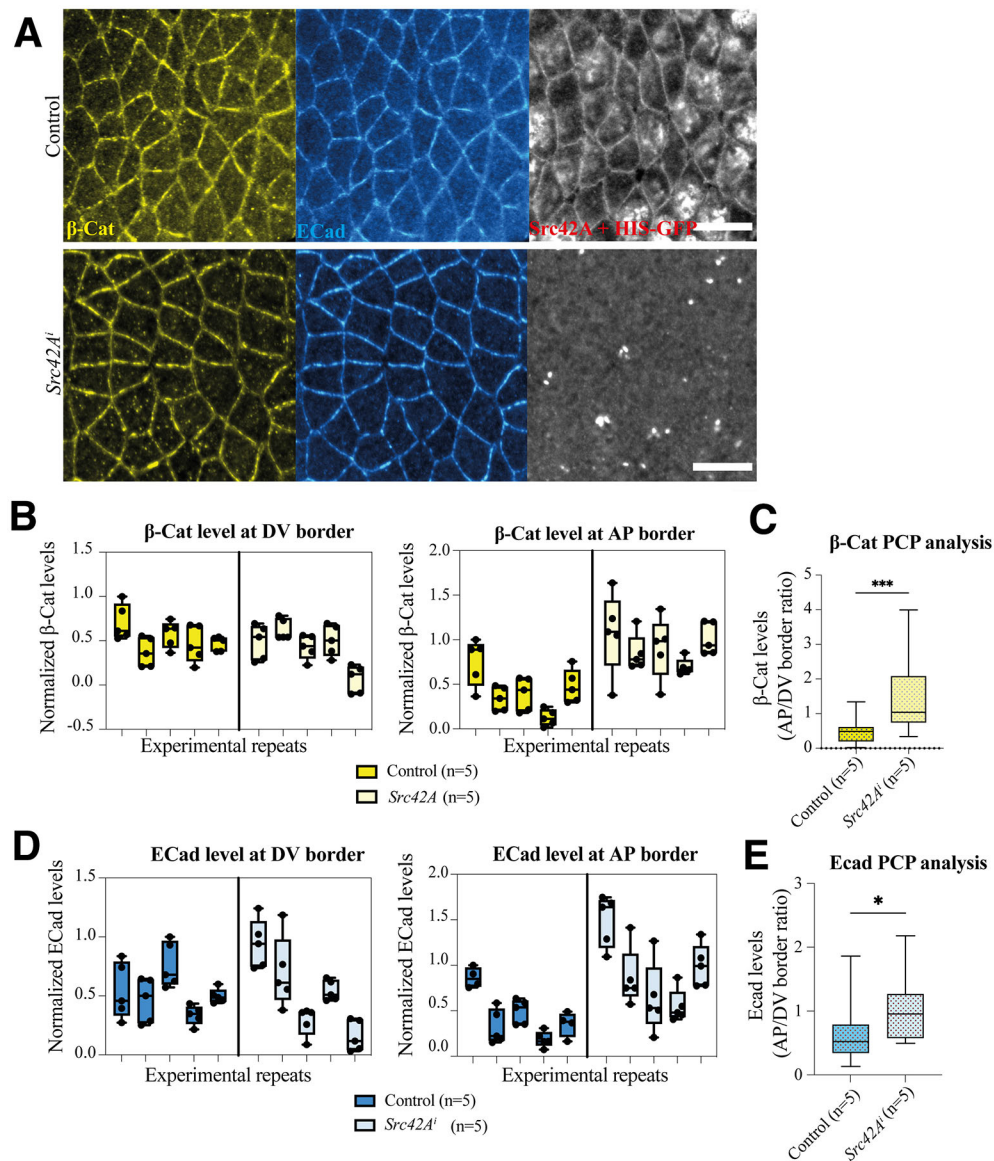


**Fig. 6. Planar polarized distribution of  $\beta$ -catenin and E-cadherin.** (A) The apical area of germband cells in fixed control and *Src42A<sup>i</sup>* embryos stained for  $\beta$ -catenin ( $\beta$ -Cat, yellow), E-cadherin (E-cad, blue) and Src42A (Src42A and His-GFP were imaged on the same channel, grey). Scale bars: 10  $\mu$ m. The staining for  $\beta$ -Cat looks more blurred and more dispersed in the control due to the fixation method applied, which, in this case, maintains cytoplasmic  $\beta$ -Cat staining and slightly obscures the junctional pool of the protein. (B,D) Quantifications of  $\beta$ -Cat and E-cad at the DV border and AP border of bAJs. Each measurement of the AP and DV interfaces was conducted on the same four-cell group. Immunostaining intensities were measured in at least five bAJs for each embryo (indicated as black dots in the graphs;  $n$ =the number of embryos analysed). Nested  $t$ -test were performed on all data; for  $\beta$ -Cat,  $P=0.4236$  at the DV border and  $P=0.0037$  at the AP border; for E-Cad,  $P=0.9700$  at the DV border and  $P=0.0499$  at the AP border.

(C,E) Planar polarity analysis of  $\beta$ -Cat and E-cad. The AP/DV border ratio show a significant difference between control and *Src42A<sup>i</sup>*. Paired Student's  $t$ -tests were performed ( $P=0.0001$  for  $\beta$ -Cat and  $P=0.0338$  for E-cad;  $n$  indicates the number of embryos analysed). The boxes indicate the interquartile range; whiskers indicate the range of the minimum and maximum values; the horizontal lines indicate the median.

(Fig. 8B-D). The prolonged residence times and accumulation of E-cadherin at the junctions could be a result of alterations in the turnover rates of E-cadherin. We therefore performed fluorescence recovery after photobleaching (FRAP) experiments on control and *Src42A<sup>i</sup>* embryos expressing E-cadherin-GFP (Fig. S7). The data show that the E-cadherin-GFP fluorescence recovery rates at tAJs in *Src42A<sup>i</sup>* are similar to controls (Fig. 8E,F). In the case of bAJs, E-cadherin-GFP recovery is initially unimpaired, but  $\sim 110$  s after bleaching, fluorescence intensity in *Src42A<sup>i</sup>* overshoots the levels of the controls, which run into equilibrium (Fig. 8E,F). The observed increase in *Src42A<sup>i</sup>* embryos is consistent with the accumulation of E-cadherin at bAJs: when E-cadherin recovery approached equilibrium in controls, E-cadherin-GFP levels further increased in *Src42A<sup>i</sup>* embryos. Furthermore, stage 7 *Sdk<sup>i</sup>* embryos were subjected to immunostaining experiments to examine E-cadherin and Src42A localization (Fig. 8G). The results show that there were no changes in E-cadherin levels, however, Src42A levels at the tAJs were increased (Fig. 8H,I). Together, these data suggest that E-cadherin turnover at adherens junctions is compromised after Src42A RNAi knockdown.

### Src42A germline clone analysis confirms the *Src42A<sup>i</sup>* phenotypes

The use of transgenic RNAi to knock down maternal Src42A has caveats, including off-target effects and incomplete depletion due to perdurance of maternal Src42A gene product. Attempts to confirm the specificity of the RNAi knockdown by rescuing *Src42A<sup>i</sup>* embryos using Src42A transgenes were inconclusive, because Src42A overexpression, in particular of tagged versions, can induce lethality (Fig. S8) (Irby and Yeatman, 2000). Therefore, to confirm the specificity of the effects caused by RNAi knockdown experiments, we generated germline clones by inducing double-strand breaks at a chromosomal site (*stlk*; 41A3) proximal to the *Src42A* (42A6-7) locus using CRISPR-Cas9 (Allen et al., 2021). In germline clones homozygous for the complete loss-of-function allele *Src42A<sup>26-1</sup>* (named *Src42A<sup>GLC</sup>* in this study), the cytoplasmic clearing was consistently defective during the transition from cell cycle 13 to 14. The number of nuclei in blastoderm stage embryos during cellularization was reduced in *Src42A<sup>GLC</sup>* embryos compared with controls, suggesting that nuclei dropping is more severe under these conditions (Fig. S9A,B, Movie 5). These defects suggest that Src42A

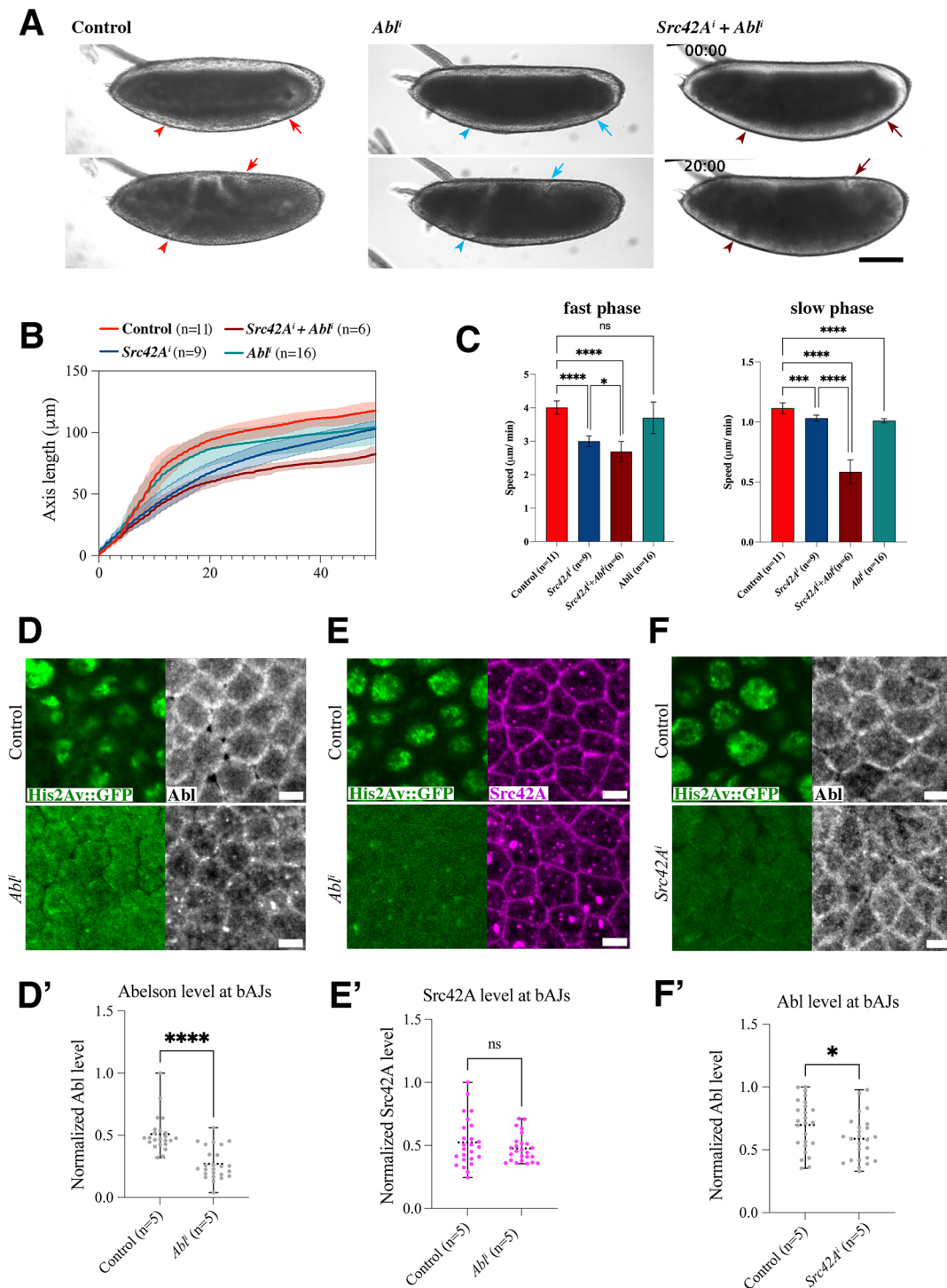


Fig. 7. See next page for legend.

may have a yet unknown function in blastoderm development. The shape and size of eggs derived from *Src42A* germline clones were more irregular and smaller, respectively, compared with *Src42A<sup>i</sup>* or wild type (Fig. 9A,C). In ovaries from *Src42A<sup>GLC</sup>*-carrying females, Src42A is absent from nurse cell interfaces. The absence of Src42A from the germline also affected the localization of E-cadherin at the nurse cell boundaries (Fig. 9B). We conclude that depletion of Src42A in the germline affects the structure of the egg chamber in oogenesis and blastoderm formation in embryogenesis.

We further analysed the speed of germband elongation (Fig. 9C,D) and the planar polarized distribution of  $\beta$ -catenin and E-cadherin (Fig. 9E-I). In all aspects examined, the phenotype of *Src42A<sup>GLC</sup>* was stronger compared with *Src42A<sup>i</sup>*, confirming the notion that some Src42A maternal gene products escaped the RNAi knockdown. This is also consistent with an increased lethality of *Src42A<sup>GLC</sup>* embryos compared with *Src42A<sup>i</sup>* (Fig. S9C). This experiment provides evidence that the knockdown effects in *Src42A<sup>i</sup>* are specific to reduction of Src42A and indicates that



**Fig. 7. Effect of Src42A and Abelson double knockdown on germband extension.** (A) Still images of bright-field timelapse video microscopy of control, *Abf<sup>l</sup>* and *Src42A<sup>i</sup>+Abf<sup>l</sup>* embryos indicate progressive delay in germ band extension (time points in min:sec). The arrowheads and the arrows indicate the anterior and posterior borders of the germband, respectively. (B) Cumulative displacement of germband cells is plotted over time for control, *Abf<sup>l</sup>*, *Src42A<sup>i</sup>* and *Src42A<sup>i</sup>+Abf<sup>l</sup>* embryos. Error bar clouds represent s.d. (C) The slopes of the curves in B were calculated for the fast and slow phase of germband extension in control, *Src42A<sup>i</sup>*, *Abf<sup>l</sup>* and *Src42A<sup>i</sup>+Abf<sup>l</sup>* embryos (slope values indicate the speed differences between the respective genotypes). A one-way ANOVA test revealed \*\*\*\* $P < 0.0001$  for *Src42A<sup>i</sup>* and *Src42A<sup>i</sup>+Abf<sup>l</sup>* versus control, and  $P = 0.0717$  for *Abf<sup>l</sup>* (ns, not significant). In slow phase, \*\*\* $P = 0.0008$  for *Src42A<sup>i</sup>*, and \*\*\*\* $P < 0.0001$  for *Src42A<sup>i</sup>+Abf<sup>l</sup>* and *Abf<sup>l</sup>* versus control. Paired Student's *t*-tests were also performed on fast and slow phase of *Src42A<sup>i</sup>* and *Src42A<sup>i</sup>+Abf<sup>l</sup>* embryos (\* $P = 0.0215$  and \*\*\*\* $P < 0.0001$ , respectively). Error bars indicate inferential values based on 95% CI (confidence interval). (D) Confocal images of the apical area of germband cells from control and *Abf<sup>l</sup>* fixed embryos stained for Abl. (D') Quantification of Abl protein levels at the bAJs in stage 6 control and *Abf<sup>l</sup>* embryos (paired Student's *t*-test; \*\*\*\* $P < 0.0001$ ). (E) Confocal images of the apical area of germband cells from control and *Abf<sup>l</sup>* fixed embryos stained for Src42A. (E') Quantification of Src42A protein level at the bAJs in stage 7 control and *Abf<sup>l</sup>* embryos (paired Student's *t*-test;  $P = 0.2907$  (ns, not significant)). (F) Confocal images of the apical area of germband cells from control and *Src42A<sup>i</sup>* fixed embryos stained for Abl. (F') Quantification of Abl protein level at the bAJs in stage 7 control and *Src42A<sup>i</sup>* embryos (paired Student's *t*-test; \* $P = 0.0473$ ). His2Av::GFP embryos were used as controls and immunolabeled in the same reaction tube as the knockdown embryos. Error bars in D', E', F' indicate the range of the minimum and maximum values. Scale bars: 100  $\mu$ m in A; 3  $\mu$ m in D, E, F.

Src42A is also involved in normal germline and blastoderm development.

## DISCUSSION

In this study, we aimed to understand the function of Src42A in regulating the dynamics of E-cadherin at adherens junctions during germband extension. Depletion of maternal and zygotic Src42A by RNAi knockdown resulted in defects in early embryogenesis. We also generated, for the first time, germline clones for a mutant Src42A allele using a CRISPR/Cas9 approach that can be used to generate germline or somatic mosaic clones for genes that are present proximal to the FRT site in the centromeric region. The embryos derived from Src42A germline clones recapitulate the phenotypes of Src42A knockdown experiments and extend the spectrum of requirements of maternal Src42A to oogenesis and blastoderm formation.

The most penetrant and robust phenotype of Src42A knockdown and maternal mutant embryos was a strongly compromised germband extension, which was associated with impaired planar polarity of E-cadherin and  $\beta$ -catenin. In particular, the E-cadherin intensity at AP cell borders was abnormally high, suggesting that E-cadherin turnover at the AP border is affected. During this stage, E-cadherin polarity was shown to control the flow of actomyosin to the AP cell border (Levayer and Lecuit, 2013). In the absence of E-cadherin endocytosis, the MyoII flow required for vertical junction constriction may be compromised. This conclusion is consistent with reduced Myo II polarity (Tamada et al., 2021) and with the reduced recoil velocity that we observed in *Src42A<sup>i</sup>* embryos when the AP border was ablated. Less tension at the AP border implies that the constriction rate of vertical AJs during the T1 transition is compromised. Our findings support the view that Src kinases (both Src42A and Src64B) act downstream of Toll-2 and Toll-6 receptors, and thereby alter the formation of Myo II cables at the AP cell border and Bazooka localization at the DV cell border (Tamada

et al., 2021). Therefore, knocking down Src42A alters the dynamics of molecular components in T1 transition cells and thereby compromises the speed of germband extension.

Previous studies on Abelson kinase (Abl) show that it affects the planar polarity of  $\beta$ -catenin during rosette formation (Tamada et al., 2012). During cell invasion, Src42A can act upstream of Abl and there is a potential feedback from Abl, with a positive impact on Src42A (Singh et al., 2010). Despite the known interplay between Src and Abl kinases, the relationship between these two kinases was not studied during germband elongation. Here, we show that RNAi knockdown of both Src42A and Abl kinases resulted in an enhanced phenotype during the slow phase of germband extension. Although the molecular details of this genetic interaction remain to be determined, our data support the model that Src42A acts upstream of Abl in a common genetic pathway in particular during the slow phase, where the rosettes resolve by extending new horizontal junctions.

Abl is required for the mobility of Canoe (the *Drosophila* homolog of afadin) from tAJs to bAJs, and this mobility depends on tyrosine phosphorylation of Canoe by Abl, as a Canoe phospho-mutant displayed delayed T1 transitions (Yu and Zallen, 2020). Canoe maternal mutants show similar defects to *Src42A<sup>i</sup>* embryos: both display less phosphotyrosine signal at the tAJs. Src42A can also phosphorylate the LIM domain-only protein Smallish, which is required for the planar polarity of Baz and Canoe at the bAJs, and Smallish is enriched at tAJs during germband extension stages (Beati et al., 2018). It is known that Canoe acts as linker between the junctional cadherin-catenin complex and the actin cytoskeleton. We hypothesize that Src42A might activate Abl and therefore lead to an enhancement of Canoe mobility. When Abl alone was knocked down, the mobility of Canoe at the AJs was impaired (Yu and Zallen, 2020). If Src42A acts directly on Canoe or indirectly through Abl to mobilize Canoe between bAJs and tAJs, this would result in a change in the proportions of Canoe at tAJs and bAJs in Abl/Src42A double knockdowns. In mammals, Afadin regulates E-cadherin turnover at cell junctions by trans-interacting with Nectin. If there is no trans-interaction, E-cadherin is internalized by Clathrin-mediated endocytosis (de Beco et al., 2009; Hoshino et al., 2005; Takeichi, 2014). In our analysis, we find that E-cadherin intensity at tAJs remains high in *Src42A<sup>i</sup>* embryos compared with wild-type embryos. This implies that E-cadherin is accumulating at the tAJs, which could possibly occur due to reduced levels of Canoe causing increasing E-cadherin clusters at the tAJs during T1 transition.

At the mid-stage of germband extension, E-cadherin protein levels at the tAJs exhibit an accumulation and dispersion cycle that correlates with cell intercalation (Vanderleest et al., 2018). The resident tricellular junction protein Sdk regulates E-cadherin endocytosis during genitalia rotation, where cell intercalation occurs continuously (Uechi and Kuranaga, 2019). Sdk connects to the actin cytoskeleton through Canoe and Polychaetoid, which transmit tension at the tAJs (Letizia et al., 2019). In *Src42A<sup>i</sup>* embryos, E-cadherin intensity is continuously increased at tAJs during cell intercalation, suggesting a specific role for Src42A in maintaining E-cadherin turnover in tAJs. What acts upstream of Src42A at tAJs in mediating E-cadherin turnover remains elusive. We aimed to understand the relationship between Sdk and Src42A in the context of E-cadherin turnover. Under *Sdk<sup>i</sup>* conditions, we were not able to observe any difference in E-cadherin intensity in fixed embryos but the level of Src42A was increased at tAJs. These data suggest that Sdk directly or indirectly controls the recruitment of Src42A to the tAJs, but the exact relationship between Sdk, Src42A and E-cadherin turnover remains to be addressed.

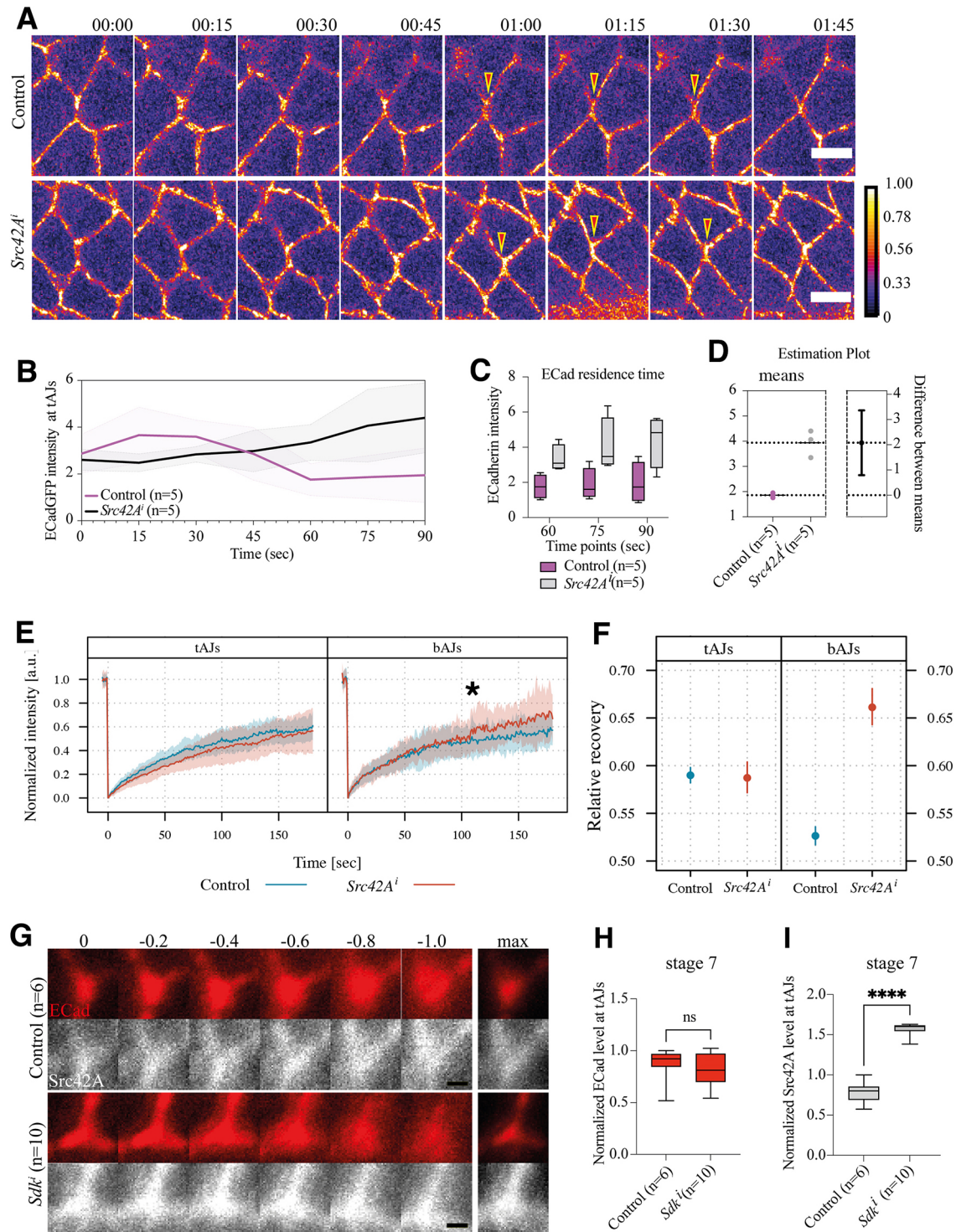


Fig. 8. See next page for legend.

In this study, we provide evidence of a requirement for Src42A in regulating molecular components at the bAJs and tAJs in axis extension in *Drosophila*. During T1 transitions, Src42A regulates the residence time of E-cadherin, suggesting that Src42A may function at the tAJs. Such a role of Src42A had not been reported so far. For example, Src42A might be involved in transducing a signal in response to mechanical tension at the tAJs into the cell. Given the reciprocal interactions between actomyosin planar

polarization and E-cadherin stabilization, we propose that, in addition to translating the planar polarized information of Toll receptors to MyoII, Src42A may affect E-cadherin dynamics at bAJs and tAJs through phosphorylation of additional, yet unknown components, which may or may not include the E-cadherin/catenin complex itself. It will therefore be interesting to identify tAJ-resident proteins that act upstream and downstream of Src42A.

**Fig. 8. Src42A controls E-cadherin turnover at AJs.** (A) Maximum intensity projection of five individual image slices with an interval of 0.3  $\mu\text{m}$  between them. Control and *Src42A<sup>i</sup>* show E-cadherin (E-Cad) levels during T1 transition were analysed using maximum intensity projection images; intensity scale bar indicates the level of E-Cad immunofluorescence (timepoints shown at the top of the images are in min:sec format; arrowheads indicates tAJs). (B) E-Cad fluorescence intensity at tAJs was normalized to bAJ intensity and background, and plotted over time [controls (magenta) and *Src42A<sup>i</sup>* (black)]. Error bar clouds indicate the s.d. (C) The intensity at the last three timepoints plotted between control (magenta) and *Src42A<sup>i</sup>* (grey). The boxes indicate the interquartile range; whiskers indicate the range of the minimum and maximum values; the horizontal lines indicate the median. (D) An unpaired *t*-test was performed with Welch's correction ( $P=0.0190$ ) indicating significant differences between means of E-Cad residence time in control and *Src42A<sup>i</sup>* embryos. (E) FRAP of E-cadherin-GFP in control (blue) and *Src42A<sup>i</sup>* (red) embryos (see Fig. S7 for further details). Germband cells in stage7/8 were photobleached at bAJs and tAJs, and mean values ( $\pm$ s.d.) of the fluorescence intensity were plotted against the time. Error bar clouds indicate s.d. There is a step-like increase in fluorescence in bAJs in *Src42A<sup>i</sup>* embryos (asterisk). (F) The plots show 95% confidence intervals based on the nonlinear weighted least-square model. Although we did not run a statistical test on these data, the clear separation of confidence intervals indicates significant differences. (G) E-Cad and Src42A immunofluorescence labelling of tAJ in control and *Sdk<sup>1</sup>* embryos at stage 7. The vertex intensity was imaged in six slices from the surface at an interval of 0.2  $\mu\text{m}$  (indicated at the top of the panels). The maximum intensity projection (max) obtained from consecutive z-stacks is shown ( $n$ =number of embryos). (H,I) Quantitative analysis of normalized E-Cad (H) and Src42A (I) levels. Unpaired Student's *t*-test shows no difference ( $P=0.1746$ ) between the control and *Sdk<sup>1</sup>*, whereas Src42A levels at the tAJs are increased in *Sdk<sup>1</sup>* embryos ( $***P=0.0001$ ). The boxes indicate the interquartile range; whiskers indicate the range of the minimum and maximum values; the horizontal lines indicate the median. Scale bars: 5  $\mu\text{m}$  in A; 0.5  $\mu\text{m}$  in G.

## MATERIALS AND METHODS

### Molecular biology and antibody generation

Full-length *Src42A* cDNA was cloned into *pGGWA* vector using the Gateway cloning method (Katzen, 2007) for antibody generation. The final *pGGWA+Src42A* vector contains a GST (Glutathione S-transferase) tag at the N-terminal end of *Src42A*; furthermore, the recombinant protein *GST-Src42A* was expressed in *BL21(DE3) E. coli* cells at 18°C overnight and purified using affinity chromatography (using Glutathione Sepharose beads). Guinea pigs were used for antibody generation (Eurogentec). After immunization, the serum from the final bleed was used directly as a *Src42A* primary antibody with a dilution of 1:500 for all experiments.

### Fly genetics

All fly stocks were raised at 25°C. To analyse the dynamic localization of *Src42A* during cellularization and germband extension, embryos from *Sqh::KI-GFP* flies were fixed and stained. Additionally, *Src42A<sup>26-1</sup>* flies (zygotic mutant) (Takahashi et al., 2005) were used to study the specificity of the generated antibody. To check the cross-reactivity of *Src42A* antibody with *Src64B*, *UASp>Src42A-HA* and *UASp>Src64B-HA* female flies (gifts from Andreas Wodarz, University of Cologne, Germany) were crossed with *engrailed>Gal4* male flies.

Maternal and zygotic knockdown of *Src42A* was performed using the *UAS/GAL4* system (Brand and Perrimon, 1993; Staller et al., 2013). Female flies carrying *shrRNA* for *Src42A* under the control of *UAS* promoter ( $y^1$  sc\*  $v^1$  sev<sup>21</sup>; P{TRiP.HMC04138}attP2/TM3, Sb<sup>1</sup>) were crossed to male driver flies ( $y^1$  w\*; P{mat $\alpha$ 4-GAL4-VP16}67; P{mat $\alpha$ 4-GAL4-VP16}15). In the next generation P{mat $\alpha$ 4-GAL4-VP16}67/+; P{mat $\alpha$ 4-GAL4-VP16}15/P{TRiP.HMC04138}attP2 flies were collected and both males and females from these genotypes were crossed to obtain embryos in which maternal and zygotic *Src42A* (named *Src42A<sup>i</sup>* in this work) was knocked down in the F2 generation. As controls in germband elongation assays, male driver lines ( $y^1$  w\*; P{mat $\alpha$ 4-GAL4-VP16}67; P{mat $\alpha$ 4-GAL4-VP16}15) were crossed to  $w^{1118}$  females, the F1 generation was backcrossed and the F2 embryos were analysed. For all immunostaining quantification experiments, *His-GFP* embryos were used as a control and stained together in a same tube

along with *Src42A<sup>i</sup>* embryos. For dynamic analysis of T1 transitions,  $y^1$  w\*; P{mat $\alpha$ 4-GAL4-VP16}67 sqh::Utrophin-GFP; P{mat $\alpha$ 4-GAL4-VP16}15/TM6 flies were used as a driver to obtain *Src42A<sup>i</sup>* embryos; *Sqh::Utrophin GFP* flies were used as a control.

For E-cadherin vertex intensity analysis and laser ablation experiments,  $y^1$  w\*; P{mat $\alpha$ 4-GAL4-VP16}67 Shg::DECadGFP/ Shg::DECadGFP; P{mat $\alpha$ 4-GAL4-VP16}15/P{TRiP.HMC04138}attP2 flies were crossed to obtain *Src42<sup>i</sup>* embryos along with an E-cadherin marker; Shg::DECadGFP flies were used as a control. For *Src42A* and *Abelson* double knockdown (*Src42A<sup>i</sup>-Abl<sup>i</sup>*) P{TRiP.HMC05140}attP40; P{TRiP.HMC04138}attP2/TM3, Sb<sup>1</sup> females were crossed with same maternal driver line as mentioned above. RNAi experiments were also performed for *sidekick (sdk)* using  $y^1$  sc\*  $v^1$  sev<sup>21</sup>; P{TRiP.HMS00292}attP2 fly line (mentioned as *Sdk<sup>i</sup>*). All the TRiP fly lines were generated at Harvard Medical School for the Transgenic RNAi Project (Ni et al., 2011).

Germ-line clones lacking *Src42A* were generated using a CRISPR-Cas9 approach based on gRNA-induced double-strand (ds) breaks at a site (*stlk* locus; 41A3) proximal to the *Src42A* (42A6-7) locus. A transgene constitutively expressing *stlk* gRNA (*P{TKO.GS00956}attP40(y<sup>+</sup>)*; Bloomington 76505) was recombined with *Src42A<sup>26-1</sup>*. To induce ds breaks in the non-essential *stlk* gene,  $y$  w; *stlk-gRNA-attP40(y<sup>+</sup>) Src42A<sup>26-1</sup>* females were crossed with  $y$  w *act5c-Cas9 lig4/Y; FRT42D ovoD(w<sup>+</sup>)/+ males. All eggs produced by F1 females of the genotype  $y$  w *act5c-Cas9 lig4 / y w; *stlk-gRNA-attP40(y<sup>+</sup>) Src42A<sup>26-1</sup> / FRT42D ovoD(w<sup>+</sup>)* are derived from germline cells lacking the dominant female-sterile *ovoD* transgene (Chou and Perrimon, 1996) and are therefore homozygous for *Src42A<sup>26-1</sup>*. Control females carrying the *FRT42D ovoD(w<sup>+</sup>)* chromosome in the absence of the *act5c-Cas9* source or of the *stlk-gRNA* source did not lay any eggs. Females carrying *Src42A<sup>26-1</sup>* germline clones were crossed with  $w^+Y$ ; *Src42A<sup>26-1</sup>/CyO[twi::GFP]* males to obtain embryos lacking maternal and zygotic *Src42A*. The genotypes of the germline clone embryos were identified by the absence of *twi::GFP* expression.**

### Immunostaining and immunoblotting

Embryos were collected from 0 to 7 h and fixed using 4% formaldehyde made in phosphate-buffered saline as described previously (Müller, 2008). After fixation, the embryos were blocked in 5% BSA and stained with the following primary antibodies: guinea pig anti-*Src42A* (1:500), rabbit anti-Bazooka (1:2000) (Wodarz et al., 1999), mouse anti-phosphotyrosine (PY20) (1:1000) (BD Biosciences, 610000), rabbit anti- $\beta$  galactosidase (1:1000) (Cappel/ICN/MP 55976), rat anti-E-cadherin DCAD2 (1:20) (Developmental Studies Hybridoma Bank), mouse anti-Arm N2 (1:250) (Developmental Studies Hybridoma Bank), rat anti-haemagglutinin 3F10 (1:1000) (Roche) and rabbit anti Abl (1:50) (a gift from Mark Peifer, University of North Carolina, Chapel Hill, USA). The following secondary antibodies were used, goat anti-guinea pig Alexa 647 (Invitrogen A-21450), goat anti-rabbit Cy3 (Strattech BS-0432R-CY3-BSS), donkey anti-mouse Cy3 (Jackson ImmunoResearch 715-165-150), donkey anti-rat Cy2 (Jackson ImmunoResearch 715-225-153) and donkey anti-rat Cy3 (Jackson ImmunoResearch 715-165-153). All secondary antibodies were used at 1:250 dilution.

For immunoblotting experiments, staged embryos were collected and lysates were prepared under denaturing conditions using 2 $\times$ SDS sample buffer [0.125 M Tris (pH 6.8), 20% glycerol, 4% SDS, 0.004% bromophenol blue and 10%  $\beta$ -mercaptoethanol]. To check the knockdown efficiency, embryos were collected from 0 to 7 h, protein lysates were prepared using RIPA buffer (50 mM Tris, 150 mM NaCl, 1% NP40, 0.1% SDS, 0.5% Na-deoxycholate and 1% Triton X-100) under non-denaturing conditions and separated on a 15% SDS-PAGE gel (Wodarz, 2008), transferred onto nitrocellulose membrane (Amersham Proton 0.2  $\mu\text{m}$  NC), and the membrane blocked and stained using the primary antibodies guinea pig anti-*Src42A* (1:500, this study), rabbit anti-haemagglutinin (1:1000) (Sigma-Aldrich H6908) and mouse anti-alpha tubulin 12G10 (1:2000) (Developmental Studies Hybridoma Bank). The secondary antibodies donkey anti-guinea pig IR dye 800 (1:10,000) (LI-COR 925-32411), donkey anti-mouse IR dye 680 (1:10,000) (LI-COR 926-68072) and donkey anti-mouse HRP (1:2000) (Jackson ImmunoResearch 715-035-150) were used to detect the

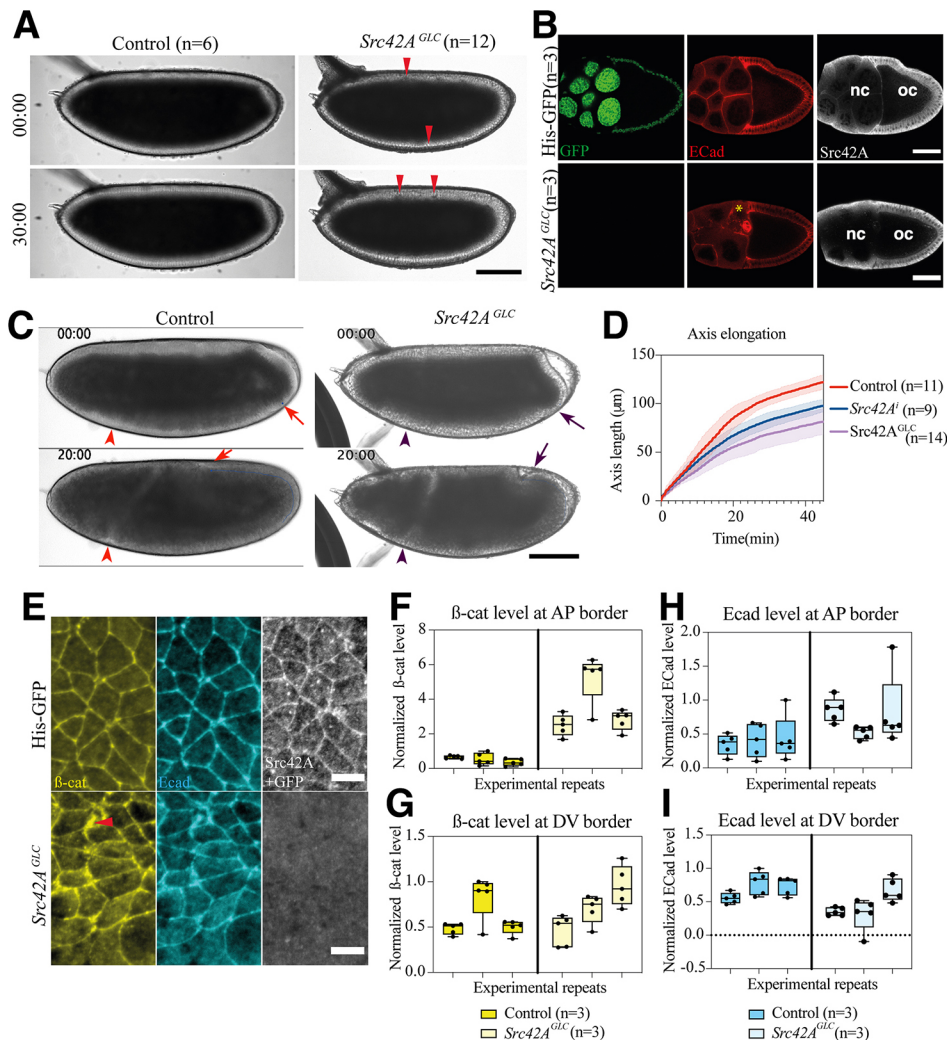


**Fig. 9. Phenotypic analyses of *Src42A* germline clones.** (A) Bright-field images of control and *Src42A<sup>GLC</sup>* embryos. Cytoplasmic clearing defects are marked by red arrowheads. (B) Stage 9 control and *Src42A<sup>GLC</sup>* egg chambers stained for E-Cad and *Src42A* (asterisk marks the difference in E-Cad distribution in nurse cells). *Src42A* antibody staining is absent from the germline (nc, nurse cells; oc, oocyte). (C) Still images taken from bright-field movies of control and *Src42A<sup>GLC</sup>* embryos. The extent of the germband is indicated by arrowheads (anterior end) and arrows (posterior end); red, control; purple, *Src42A<sup>GLC</sup>*. (D) Germband elongation is plotted over time for *Src42A<sup>GLC</sup>* in comparison with control and *Src42A<sup>i</sup>* conditions. The s.d. is shown as error bar clouds. (E) Control and *Src42A<sup>GLC</sup>* embryos were fixed and stained for  $\beta$ -Cat and E-Cad; representative stage 7 embryos are shown (red arrowhead indicates a defect in  $\beta$ -Cat distribution). (F-I) Normalized  $\beta$ -Cat and E-Cad levels at the AP and DV germband cell interfaces were calculated and plotted to compare control and *Src42A<sup>GLC</sup>* embryos. Nested *t*-test were performed on all data;  $P=0.6183$  for  $\beta$ -Cat at DV border and  $P=0.0268$  at AP border;  $P=0.1380$  for E-Cad at DV border and  $P=0.0370$  at AP border. The boxes indicate the interquartile range; whiskers indicate the range of the minimum and maximum values; the horizontal lines indicate the median. Scale bars: 100  $\mu$ m in A,C; 50  $\mu$ m in B; 5  $\mu$ m in E.

protein levels in a LI-COR Odyssey Fc imaging system. The immunoblots were simultaneously stained with antibodies against the antigen to be detected and with anti-alpha tubulin as a loading control. The immunoblot was imaged in two separate channels and is depicted in two panels.

## Image acquisition and quantification

### Protein levels at bicellular and tricellular AJs

Images were acquired using confocal laser scanning microscope (Zeiss LSM880) for 1.2  $\mu$ m depth from the surface in *z*-plane with 0.2  $\mu$ m interval. All the images were processed and analysed using Fiji. In total, six images were acquired, and maximum intensity projection (MIP) images were generated from these images. Using the MIP images, quantifications were performed. Average pixel intensity at the two and three cell contacts were measured and subtracted with the background value. The pixel intensities were normalized to the maximum value of the control image. Both control and *Src42A<sup>i</sup>* embryos were stained in the same tube for quantification purposes. The planar polarized distribution of immunolabeled proteins was analysed by measuring pixel intensities of bicellular junctions at AP and DV borders; these pixel intensities were normalized to the maximum value of AP- and DV-border measurement in control embryos. The ratios of AP- to DV-border were calculated by dividing the raw data of DV-border measurement to AP-border measurements.

### Germband elongation assay

Bright-field images were taken from Zeiss Axiophot and Olympus BX61 microscope, and processed using Fiji. The length of germband elongation

was tracked using ‘manual tracking’ plug-in, and the cumulative displacement of germband were plotted over time. To access the speed of germband elongation, a linear curve was drawn for the slow and fast phase of germband elongation, and the linear curve slope was calculated for respective phases.

### T1 transition analysis

Live-imaging experiments were performed using *sqh::Utrophin-GFP* as a marker for cell membrane. Imaging was performed using a confocal laser scanning microscope (LSM880) in airy scan mode. The transition between stage 6 and 7 were recorded with a 15 s time interval. All the acquired images were analysed using ‘Tissue Analyzer’ plug-in in Fiji. Images from each timepoints were segmented and the length of AP axis and DV axis was measured from segmented images. Initial AP axis length ( $L_0$ ) is normalized to the length over time ( $L_t$ ) and the normalized value was plotted over time.

### E-cadherin vertex intensity ratio

Images were taken using a confocal laser scanning microscope in airy scan mode. Germband cells undergoing T1 transitions were imaged for a depth of 1  $\mu$ m in *z*-plane with 0.2  $\mu$ m interval. MIP images were generated from the acquired images for all time points. Cells undergoing T1 transition containing 2.5  $\mu$ m AP axis length were selected and used for analysis. From the final images, E-cadherin vertex intensity ratio is calculated using the following formula ( $(I_{AJs-IB})/(I_{BAs-IB})$ ) (Vanderleest et al., 2018). The vertex intensity ratio was then plotted over time.

### Statistical methods

Various types of statistical tests were applied and indicated in the figure legends. When a paired Student's *t*-test was performed, the normal distribution of the data was calculated using D'Agostino and Pearson test for datasets with more than eight elements (D'Agostino and Pearson, 1973). Alternatively, the Kolmogorov–Smirnov Test was used (Smirnov, 1948). The sample sizes (*n*) for each experiment are indicated in the figure legends.

### Fluorescence recovery after photobleaching (FRAP) experiments

Stage 7 embryos were mounted on glue-covered coverslips. Movies were acquired with a Leica SP8 equipped with a 40×/1.3 NA oil immersion objective using the FRAP wizard of the LAS X software with a speed of 400 lines/s and 8× zoom at 256×256 pixel resolution and 1 s intervals. For each embryo, five pre-bleach and 181 post-bleach frames were recorded. Regions were point-bleached with 100% laser intensity for 250 ms. Bleached regions were afterwards tracked manually to correct cell movement, and intensities were measured in a circle with a radius of 3 pixels. Raw measurements were corrected for background fluorescence and continuous photobleaching, and normalized by setting pre-bleach values to 1 and the first post-bleach value to 0. Parameters *A* and  $\tau$  of an exponential model of the form:

$$f_A, \tau(t) = A \cdot (1 - e^{-t/\tau}) \quad (1)$$

were fitted to the values numerically using a weighted non-linear least square approach with the *nls* function of the R statistical software package (v4.1). The reciprocal of the variance for each timepoint was used as a weight. 95% confidence intervals for *A* and  $\tau$  were determined using the MASS::confint.nls function. Confidence intervals for the half-recovery time were calculated from the interval for  $\tau$ .

### Laser ablation

Stage 7 embryos expressing ECadGFP were prepared for live imaging and recorded in the GFP channel with 1 s time interval on a confocal laser scanning microscopy (Zeiss, LSM980 with 100× magnification using oil immersion, 1.4 NA). A 355 nm pulsed laser (DPSL355/14, 355 nm, 70 μJ/pulse, Rapp OptoElectronic) was employed for ablation and manipulated on the 'REO-SysCon-Zen' platform (Rapp OptoElectronic). The 355 nm pulsed laser was mounted on epipoint of the confocal laser scanning microscopy. Laser ablation was performed with 5% of laser power, with 200 ms (around 40 pulses) exposure time at the AP axis of the cells undergoing T1 transition. For analysis, the displacement length of ablated tAJs [L(*t*)] were measured manually in Fiji. The displacement value were normalized to the initial length [L(0)] between tAJs and plotted over time. The initial recoil velocity were calculated using Kelvin-Voigt fibre model to the following equations using Prism8 (Fernandez-Gonzalez et al., 2009; Liang et al., 2016).

Extraction of initial recoil velocity value was calculated as follows:

$$\varepsilon(t) = L(t) - L(0) = \frac{F_0}{E} \cdot \left( 1 - e^{-\left[\frac{E}{\mu}\right]_{st}} \right), \quad (2)$$

where  $F_0$  is the tensile force present at the junction before ablation, *E* is the elasticity of the junction and  $\mu$  is the viscosity coefficient related to the viscous drag of the cell cytoplasm.

As fitting parameters for the above equation, we introduced:

$$\text{Initial recoil} = \frac{d\varepsilon(0)}{dt} = \frac{F_0}{\mu}. \quad (3)$$

### Acknowledgements

We thank Andreas Wodarz and Mark Peifer for providing fly stocks and antibodies. We thank Tanja Wilhelm, Christine Otto and Nicole Schleinschok for fly maintenance and expert technical assistance, and Monika Winnekecht and Birgit Simon for preparing fly media. We thank the Bloomington Drosophila stock centre for *Drosophila* stocks, the Developmental Studies Hybridoma Bank for antibodies and the Transgenic RNAi Project for providing RNAi lines. Work in H.-A.J.M.'s laboratory

was supported by core funding from the Universität Kassel and the PhosMOrg Consortium.

### Competing interests

The authors declare no competing or financial interests.

### Author contributions

Conceptualization: S.A.H.B., S.L., H.-A.J.M.; Methodology: L.C., W.B., R.S., D.K., S.L., H.-A.J.M.; Validation: L.C., R.S., H.-A.J.M.; Formal analysis: L.C., R.S., D.K., S.A.H.B., H.-A.J.M.; Investigation: L.C., W.B., R.S., S.A.H.B., H.-A.J.M.; Resources: S.L., H.-A.J.M.; Data curation: H.-A.J.M.; Writing - original draft: L.C.; Writing - review & editing: L.C., S.L., H.-A.J.M.; Visualization: L.C., R.S.; Supervision: S.A.H.B., S.L., H.-A.J.M.; Project administration: S.A.H.B., H.-A.J.M.; Funding acquisition: S.A.H.B., S.L., H.-A.J.M.

### Funding

Work in S.L.'s laboratory was supported by the Deutsche Forschungsgemeinschaft [SFB 1348 (Dynamic Cellular Interfaces) and SFB 1009 (Breaking Barriers)], by the 'Cells-in-Motion' Cluster of Excellence at the Universität Münster (EXC 1003-CiM), and the Universität Münster. Work in H.-A.J.M.'s laboratory was supported by Universität Kassel 'Future programme' PhosMOrg to H.-A.J.M. and a new investigator award from the Universität Kassel to S.A.H.B.

### Data availability

All relevant data can be found within the article and its supplementary information.

### Peer review history

The peer review history is available online at <https://journals.biologists.com/dev/lookup/doi/10.1242/dev.201119.reviewer-comments.pdf>

### References

- Allen, S. E., Koreman, G. T., Sarkar, A., Wang, B., Wolfner, M. F. and Han, C. (2021). Versatile CRISPR/Cas9-mediated mosaic analysis by gRNA-induced crossing-over for unmodified genomes. *PLoS Biol.* **19**, e3001061. doi:10.1371/journal.pbio.3001061
- Ambrosini, A., Rayer, M., Monier, B. and Suzanne, M. (2019). Mechanical function of the nucleus in force generation during epithelial morphogenesis. *Dev. Cell* **50**, 197-211.e5. doi:10.1016/j.devcel.2019.05.027
- Beati, H., Peek, I., Hordowska, P., Honemann-Capito, M., Glashauser, J., Renschler, F. A., Kakanj, P., Ramrath, A., Leptin, M., Luschnig, S. et al. (2018). The adherens junction-associated LIM domain protein Smallish regulates epithelial morphogenesis. *J. Cell Biol.* **217**, 1079-1095. doi:10.1083/jcb.201610098
- Bertet, C., Sulak, L. and Lecuit, T. (2004). Myosin-dependent junction remodelling controls planar cell intercalation and axis elongation. *Nature* **429**, 667-671. doi:10.1038/nature02590
- Blankenship, J. T., Backovic, S. T., Sanny, J. S. P., Weitz, O. and Zallen, J. A. (2006). Multicellular rosette formation links planar cell polarity to tissue morphogenesis. *Dev. Cell* **11**, 459-470. doi:10.1016/j.devcel.2006.09.007
- Brand, A. H. and Perrimon, N. (1993). Targeted gene expression as a means of altering cell fates and generating dominant phenotypes. *Development* **118**, 401-415. doi:10.1242/dev.118.2.401
- Brunet, T., Bouclet, A., Ahmadi, P., Mitrossilis, D., Driquez, B., Brunet, A.-C., Henry, L., Serman, F., Béalle, G., Ménager, C. et al. (2013). Evolutionary conservation of early mesoderm specification by mechanotransduction in Bilateria. *Nat. Commun.* **4**, 2821. doi:10.1038/ncomms3821
- Chou, T. B. and Perrimon, N. (1996). The autosomal FLP-DFS technique for generating germline mosaics in *Drosophila melanogaster*. *Genetics* **144**, 1673-1679. doi:10.1093/genetics/144.4.1673
- Da Silva, S. M. and Vincent, J.-P. (2007). Oriented cell divisions in the extending germband of *Drosophila*. *Development* **134**, 3049-3054. doi:10.1242/dev.004911
- D'Agostino, R. B. and Pearson, E. S. (1973). Tests for departure from normality. Empirical results for the distributions of  $b^2$  and  $\sqrt{b^1}$ . *Biometrika* **60**, 613. doi:10.2307/2335012
- De Beco, S., Guedry, C., Amblard, F. and Coscoy, S. (2009). Endocytosis is required for E-cadherin redistribution at mature adherens junctions. *Proc. Natl. Acad. Sci. USA* **106**, 7010-7015. doi:10.1073/pnas.0811253106
- Edgar, B. A. and O'farrell, P. H. (1989). Genetic control of cell division patterns in the *Drosophila* embryo. *Cell* **57**, 177-187. doi:10.1016/0092-8674(89)90183-9
- Fernandez-Gonzalez, R., Simoes, S. M., Röper, J.-C., Eaton, S. and Zallen, J. A. (2009). Myosin II dynamics are regulated by tension in intercalating cells. *Dev. Cell* **17**, 736-743. doi:10.1016/j.devcel.2009.09.003
- Finegan, T. M., Hervieux, N., Nestor-Bergmann, A., Fletcher, A. G., Blanchard, G. B. and Sanson, B. (2019). The tricellular vertex-specific adhesion molecule Sidekick facilitates polarised cell intercalation during *Drosophila* axis extension. *PLoS Biol.* **17**, e3000522. doi:10.1371/journal.pbio.3000522

- Gheisari, E., Aakhte, M. and Müller, H.-A. J.** (2020). Gastrulation in *Drosophila melanogaster*: Genetic control, cellular basis and biomechanics. *Mech. Dev.* **163**, 103629. doi:10.1016/j.mod.2020.103629
- Hoshino, T., Sakisaka, T., Baba, T., Yamada, T., Kimura, T. and Takai, Y.** (2005). Regulation of E-cadherin endocytosis by nectin through afadin, Rap1, and p120ctn. *J. Biol. Chem.* **280**, 24095-24103. doi:10.1074/jbc.M414447200
- Irby, R. B. and Yeatman, T. J.** (2000). Role of Src expression and activation in human cancer. *Oncogene* **19**, 5636-5642. doi:10.1038/sj.onc.1203912
- Irvine, K. D. and Wieschaus, E.** (1994). Cell intercalation during *Drosophila* germband extension and its regulation by pair-rule segmentation genes. *Development* **120**, 827-841. doi:10.1242/dev.120.4.827
- Katzen, F.** (2007). Gateway<sup>®</sup> recombinational cloning: a biological operating system. *Expert Opin. Drug Discov.* **2**, 571-589. doi:10.1517/17460441.2.4.571
- Kong, D., Wolf, F. and Großhans, J.** (2017). Forces directing germ-band extension in *Drosophila* embryos. *Mech. Dev.* **144**, 11-22. doi:10.1016/j.mod.2016.12.001
- Letizia, A., He, D., Astigarraga, S., Colombelli, J., Hatini, V., Llimargas, M. and Treisman, J. E.** (2019). Sidekick is a key component of tricellular adherens junctions that acts to resolve cell rearrangements. *Dev. Cell* **50**, 313-326.e5. doi:10.1016/j.devcel.2019.07.007
- Levayer, R. and Lecuit, T.** (2013). Oscillation and polarity of E-cadherin asymmetries control actomyosin flow patterns during morphogenesis. *Dev. Cell* **26**, 162-175. doi:10.1016/j.devcel.2013.06.020
- Levayer, R., Pelissier-Monier, A. and Lecuit, T.** (2011). Spatial regulation of Dia and Myosin-II by RhoGEF2 controls initiation of E-cadherin endocytosis during epithelial morphogenesis. *Nat. Cell Biol.* **13**, 529-540. doi:10.1038/ncb2224
- Liang, X., Michael, M. and Gomez, G. A.** (2016). Measurement of mechanical tension at cell-cell junctions using two-photon laser ablation. *Bio. Protoc.* **6**, e2068. doi:10.21769/BioProtoc.2068
- Müller, H.-A. J.** (2008). Immunolabeling of embryos. *Methods Mol. Biol.* **420**, 207-218. doi:10.1007/978-1-59745-583-1\_12
- Ni, J.-Q., Zhou, R., Czech, B., Liu, L.-P., Holderbaum, L., Yang-Zhou, D., Shim, H.-S., Tao, R., Handler, D., Karpowicz, P. et al.** (2011). A genome-scale shRNA resource for transgenic RNAi in *Drosophila*. *Nat. Methods* **8**, 405-407. doi:10.1038/nmeth.1592
- Paré, A. C. and Zallen, J. A.** (2020). Cellular, molecular, and biophysical control of epithelial cell intercalation. *Curr. Top. Dev. Biol.* **136**, 167-193. doi:10.1016/bs.ctdb.2019.11.014
- Paré, A. C., Vichas, A., Fincher, C. T., Mirman, Z., Farrell, D. L., Mainieri, A. and Zallen, J. A.** (2014). A positional Toll receptor code directs convergent extension in *Drosophila*. *Nature* **515**, 523-527. doi:10.1038/nature13953
- Rauzi, M., Lenne, P.-F. and Lecuit, T.** (2010). Planar polarized actomyosin contractile flows control epithelial junction remodelling. *Nature* **468**, 1110-1114. doi:10.1038/nature09566
- Röper, J.-C., Mitrossilis, D., Stirnemann, G., Waharte, F., Brito, I., Fernandez-Sanchez, M.-E., Baaden, M., Salamero, J. and Farge, E.** (2018). The major  $\beta$ -catenin/E-cadherin junctional binding site is a primary molecular mechanotransducer of differentiation in vivo. *Elife* **7**, e33381. doi:10.7554/eLife.33381
- Salomon, J., Gaston, C., Magescas, J., Duvauchelle, B., Canioni, D., Sengmanivong, L., Mayeux, A., Michaux, G., Campeotto, F., Lemale, J. et al.** (2017). Contractile forces at tricellular contacts modulate epithelial organization and monolayer integrity. *Nat. Commun.* **8**, 13998. doi:10.1038/ncomms13998
- Singh, J., Aaronson, S. A. and Mlodzik, M.** (2010). *Drosophila* Abelson kinase mediates cell invasion and proliferation through two distinct MAPK pathways. *Oncogene* **29**, 4033-4045. doi:10.1038/onc.2010.155
- Smirnov, N.** (1948). Table for estimating the goodness of fit of empirical distributions. *Ann. Math. Statist.* **19**, 279-281. doi:10.1214/aoms/1177730256
- Staller, M. V., Yan, D., Randklev, S., Bragdon, M. D., Wunderlich, Z. B., Tao, R., Perkins, L. A., Depace, A. H. and Perrimon, N.** (2013). Depleting gene activities in early *Drosophila* embryos with the "maternal-Gal4-shRNA" system. *Genetics* **193**, 51-61. doi:10.1534/genetics.112.144915
- Sun, Z., Amourda, C., Shagirov, M., Hara, Y., Saunders, T. E. and Toyama, Y.** (2017). Basolateral protrusion and apical contraction cooperatively drive *Drosophila* germ-band extension. *Nat. Cell Biol.* **19**, 375-383. doi:10.1038/ncb3497
- Takahashi, M., Takahashi, F., Ui-Tei, K., Kojima, T. and Saigo, K.** (2005). Requirements of genetic interactions between Src42A, armadillo and shotgun, a gene encoding E-cadherin, for normal development in *Drosophila*. *Development* **132**, 2547-2559. doi:10.1242/dev.01850
- Takeichi, M.** (2014). Dynamic contacts: rearranging adherens junctions to drive epithelial remodelling. *Nat. Rev. Mol. Cell Biol.* **15**, 397-410. doi:10.1038/nrm3802
- Tamada, M., Farrell, D. L. and Zallen, J. A.** (2012). Abl regulates planar polarized junctional dynamics through  $\beta$ -catenin tyrosine phosphorylation. *Dev. Cell* **22**, 309-319. doi:10.1016/j.devcel.2011.12.025
- Tamada, M., Shi, J., Bourdot, K. S., Supriyatno, S., Palmquist, K. H., Gutierrez-Ruiz, O. L. and Zallen, J. A.** (2021). Toll receptors remodel epithelia by directing planar-polarized Src and PI3K activity. *Dev. Cell* **56**, 1589-1602.e9. doi:10.1016/j.devcel.2021.04.012
- Uechi, H. and Kuranaga, E.** (2019). The tricellular junction protein sidekick regulates vertex dynamics to promote bicellular junction extension. *Dev. Cell* **50**, 327-338.e5. doi:10.1016/j.devcel.2019.06.017
- Vanderleest, T. E., Smits, C. M., Xie, Y., Jewett, C. E., Blankenship, J. T. and Loerke, D.** (2018). Vertex sliding drives intercalation by radial coupling of adhesion and actomyosin networks during *Drosophila* germband extension. *Elife* **7**, e34586. doi:10.7554/eLife.34586
- Williams, M. L. and Solnica-Krezel, L.** (2017). Regulation of gastrulation movements by emergent cell and tissue interactions. *Curr. Opin. Cell Biol.* **48**, 33-39. doi:10.1016/j.ceb.2017.04.006
- Wodarz, A.** (2008). Extraction and immunoblotting of proteins from embryos. *Methods Mol. Biol.* **420**, 335-345. doi:10.1007/978-1-59745-583-1\_21
- Wodarz, A., Ramrath, A., Kuchinke, U. and Knust, E.** (1999). Bazooka provides an apical cue for Inscuteable localization in *Drosophila* neuroblasts. *Nature* **402**, 544-547. doi:10.1038/990128
- Yu, H. H. and Zallen, J. A.** (2020). Abl and Canoe/Afadin mediate mechanotransduction at tricellular junctions. *Science* **370**, eaba5528. doi:10.1126/science.aba5528
- Zallen, J. A. and Wieschaus, E.** (2004). Patterned gene expression directs bipolar planar polarity in *Drosophila*. *Dev. Cell* **6**, 343-355. doi:10.1016/S1534-5807(04)00060-7